Longitudinal Aberrations Caused by Optical Filters and Their Compensation in Multispectral Imaging

Johannes Brauers and Til Aach

Institute of Imaging and Computer Vision
RWTH Aachen University, 52056 Aachen, Germany
tel: +49 241 80 27860, fax: +49 241 80 22200
web: www.lfb.rwth-aachen.de

in: IEEE International Conference on Image Processing (ICIP2008). See also BIBTEX entry below.

RWTHAACHEN
RHEINISCH-WESTFÄLISCHE TECHNISCHE HOCHSCHULE AACHEN

LONGITUDINAL ABERRATIONS CAUSED BY OPTICAL FILTERS AND THEIR COMPENSATION IN MULTISPECTRAL IMAGING

Johannes Brauers and Til Aach

Institute of Imaging & Computer Vision
RWTH Aachen University
52056 Aachen
Phone: +49(0)241-80-27866
E-Mail: jb,ta@lfb.rwth-aachen.de

ABSTRACT

Multispectral cameras enable high-fidelity color image acquisition by separation of the electromagnetic spectrum with optical bandpass filters mounted on a filter wheel between optics and imaging sensor. A multispectral image is acquired by capturing one grayscale image per wheel position and combining the images afterwards. Since the optical filters differ in their thicknesses and refraction indices, both transversal (geometric distortions) and longitudinal aberrations (blurring) occur. We present a physical model for the longitudinal aberrations and describe the resulting distortion effects. This knowledge serves as a basis for our compensation algorithm, which performs a shift-variant deconvolution of the image, significantly improving the image quality. We furthermore describe a practicable calibration procedure for our algorithm.

Index Terms— multispectral imaging, deconvolution, raytracing

1. INTRODUCTION

In terms of color accuracy, multispectral cameras outperform [1] 1-chip RGB cameras since the latter ones exhibit a systematic color error and require interpolation algorithms to retrieve full color information. However, since this is acceptable for most users, the mass-produced, small and cheap RGB cameras are widely used in practice. In contrast, multispectral cameras use in the most prominent case [2, 3] expensive optical filters mounted on a computer-controlled filter wheel to achieve high color fidelity.

Although this camera type offers a very good stop-band attenuation, temperature stability and – in the case where the filters are placed between optics and sensor – a relatively small overall size (see [4]), there are some critical issues: The positioning of the optical bandpass filters in the optical path causes aberrations, since the filters exhibit different thicknesses, refraction indices and are not aligned in a fully coplanar manner due to inaccuracies in the manufacturing process. The *transversal* aberrations, i.e., the deflection of the optical rays perpendicular to the optical axis, cause a geometrical misalignment of the spectral channels which are discussed, e.g., in [4, 5].

In this paper, we analyze the *longitudinal* aberrations causing a blurred image and address both aberration types in our combined compensation algorithm. Deconvolution with respect to an additional geometric distortion is described in [6] with a shift-*in*variant PSF, which is not appropriate for our model. Also, the geometric distortion is reduced to a simple translation in a preprocessing step and therefore separated from the compensation algorithm. An algorithm in the spatial domain is presented in [7]: Here, image registration is performed with a spatially varying normalized LMS filter. However, the quadratic difference measure does not consider channel brightness changes we have to expect for multispectral channels. Also, the inconvenient zigzag-like scan-order using a Hilbert curve instead of a row-wise scan-order is a critical issue. In [8], the same application as our's is concerned: Deconvolution of multispectral images is performed with a circular and shift-invariant PSF. However, as shown in the following section, a shift-variant model is more appropriate.

We start by the derivation of our physical model in section 2 providing the basis for our calibration and compensation algorithm in section 3. The results are discussed in section 4 before we finish with conclusions in section 5.

2. PHYSICAL MODEL

A simplified model of our optical setup is depicted in Fig. 1: We simulated the rays emerging from nine object points and their clipping by the aperture at the position $z = g = 70$mm. (Only three object points are shown in the figure for convenience.) Without an optical filter, the ideal lens would refract the rays to join in exactly nine spots in the image plane; with the well-known thin lens formula the image distance without filter is $b' = \frac{gf}{g-f} = 52.5mm$.
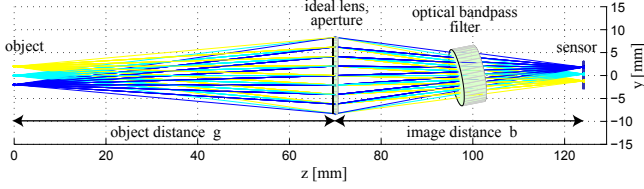
Fig. 1. Raytracing of 3 object points (y=-2,0,2 mm), f=30mm, g=70mm, b=54.15mm, filter thickness d=5mm, refraction index n_2=1.45, filter normal $\mathbf{n} = [0.19, 0.19, 0.96]$, F-number: F=1.8 ($\mathbf{r}$=8.33mm).

With the additional optical bandpass filter, the rays are refracted twice when entering and leaving the filter, resulting in a parallel shift of the rays [9]. We already investigated the resulting transversal image distortions describing the image position shift inside the image plane in [4] by simulation of the principal rays according to a pinhole camera.

In this paper, we consider a fan of rays for each object and therefore account for the focusing aspects arising with a real lens. More precisely, since the rays are shifted parallel by the filter, they do not join in a single point but instead cause a blurring spot: In this particular example, we modeled a total number of 49 rays emerging from each object point passing through different positions in the circular aperture. Without the optical filter, the 49 rays would meet in exactly one point on the sensor plane in our simulation. However, since the optical filter refracts the rays, they impinge on the sensor plane at different positions. This is illustrated by Fig. 2: Here, each box shows the raytracing result in the image plane for one object point, where each spot represents one ray. The image position b has been optimized in terms of blur spot size to focus optimally, but still the spots do not join in a single point.

Four conclusions are derived from Fig. 2: First, the kernel of the blurred spots does not resemble a typical blur disc and provides no circular symmetry; the principal ray, which passes through the center of the aperture, is instead mapped to the border of the blur shape (shown by the circle). Second, the blur kernel varies slowly over the image position, yielding a shift-variant PSF. Third, since each filter has different properties (thickness, refraction index, tilt angle), a different PSF results for each filter. Forth, the image points are spread along the tilt axis of the optical bandpass filter. To summarize, each of the seven optical bandpass filters has a unique, spatial varying and non-symmetrical PSF.

The longitudinal aberrations (blur) are therefore modeled with a spatially varying convolution. We additionally account for the transversal aberrations causing a geometric distortion of the image by incorporating a displacement vector field and derive

$$\tilde{I}_c(x_0, y_0) = \sum_{x,y} h_c(x, y; x_0, y_0) \cdot$$
$$I_c(x + d_{x,c}(x,y), y + d_{y,c}(x,y)) + n(x_0, y_0), \tag{1}$$

where I_c is the original image for spectral channel c, $\tilde{I}_c$ is the distorted image, h_c denotes the shift-variant point spread function for spectral channel c, and n is additive noise. The variables x_0, y_0 and x and y are image coordinates. The terms $d_{x,c}$ and $d_{y,c}$ represent the displacement vector field, whose model and estimation are discussed in [4].
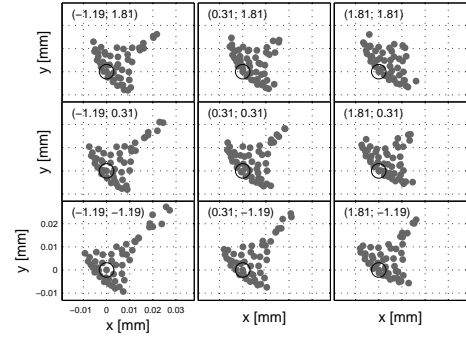

Fig. 2. Spot diagrams for 9 object points; numbers denote absolute positions of principal rays (circles); the axes' positions are relative; our optical setup is depicted in Fig. 1.

3. CALIBRATION AND COMPENSATION ALGORITHM

3.1. Calibration

For the estimation of the spatially varying PSF in Eq. (1) we use a grayscale template with random noise, e.g., a sheet printed by a grayscale laser printer. Since the spectra of the spatial locations solely differ in their brightness but not in their spectral composition, the resulting grayscale images for the available spectral channels also differ in their brightness and geometrical distortion but not in their spectral content. The brightness can be compensated in a straightforward manner, leaving the aberrations. This enables us to compare the spectral channels in terms of their geometric distortion and blur. Since one channel can be focused optimally, we select it as reference channel and adapt all other channels to it. Therefore, all further mentioned PSFs and OTFs are relative to the reference channel. Even though the calibration is not related in an absolute manner to the reference object, it can be performed with less expense. Our future plans include an absolute calibration.
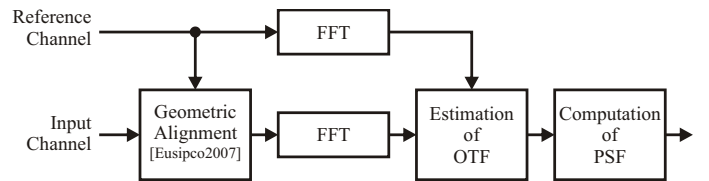

Fig. 3. Our calibration algorithm.

Since the optical filter discussed in section 2 ensures the continuity of the PSF, we estimate the *slowly* changing PSF blockwise, i.e., not for each spatial position to reduce the computational effort. Our output crossfading technique (see below) interpolates the PSF for the intermediate positions. Our calibration algorithm is illustrated in Fig. 3: The geometric alignment is performed prior to the PSF estimation as described in [4]; in brief, the reference and input channels are registered subject to an affine transformation model and match exactly after correction. The displacement vector field is retained for later acquired images and their compensation. Now the image blocks from input and reference blocks are transformed to the frequency domain and the OTFs are computed by division. The OTFs describe the relation between an input channel and the reference channel. We use a relative calibration, because the estimation of an absolute PSF/OTF is ill-posed due to the high variability of the PSFs.

3.2. Compensation

The compensation of the aberrations requires two steps. First, the spectral channels are aligned using the displacement vector field determined in the calibration part. Second, the images are deconvolved blockwise using Wiener deconvolution [10] with the corresponding PSFs, which have been estimated in advance. To suppress both blocking as well as leakage artifacts, the image blocks are embedded into two larger blocks. The first embedding extends the size of the image block to perform crossfading: the extended borders overlap with the adjacent image blocks and we apply a smooth transition function to fade from one block to its neighbor. This way, the spatially (slowly) changing PSF is taken into account. The second embedding into a still larger block is used to prevent leakage artifacts, which would be introduced by non-symmetrical blocks. Towards this end we edge-taper the extended border with a Gaussian function. The compensation is carried out for all spectral channels except the reference channel.

4. RESULTS

Our multispectral camera [4] uses seven optical bandpass filters (12.5mm$\varnothing$) from 400nm to 700nm in steps of 50nm; each filter has an optical bandwidth of 40nm, a maximum physical thickness of 7mm and the refraction indices are either 1.45 or 2.05. The internal grayscale camera Sony XCD-SX900 has a resolution of 1280×960 pixel and the lens is a Nikkor AF-S DX 18-70mm.

For our block-processing, we use a block size of 160×192 pixel, which is a good compromise between granularity and sufficient size of the blocks, also preventing fragmented blocks at the image edges; however, it is not an optimum in terms of FFT size. We apply a triangular crossfading function to fade the blocks into each other; the left and right overlap-
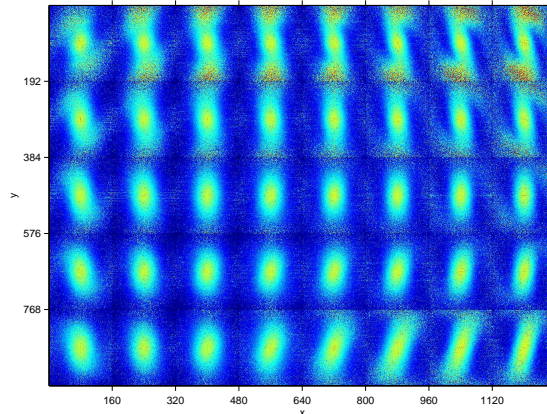

Fig. 4. MTF of image blocks for λ_{sel}=450nm spectral channel, related to λ_{ref}=550nm channel; the image positions of the blocks are denoted on the axes.

ping areas are 80 pixel wide and the top and bottom areas are 96 pixel high. To prevent leakage artifacts, we use an additional border around the image with its size identical to the crossfading border. Edge-tapering is then performed by using a Gaussian function with $[\sigma_h, \sigma_v] = [12.5, 14.9]$. The (windowed) PSF size is 15×15. For deconvolution, a noise to signal power ratio of 0.07 yielded good reconstruction results.

Fig. 4 shows the result of our blockwise MTF analysis for the spectral channel λ_{sel}=400nm, confirming the shift-variance of the MTF. Since the spectral channels have been geometrically aligned in a previous step, the maximum of the PSF is centered.
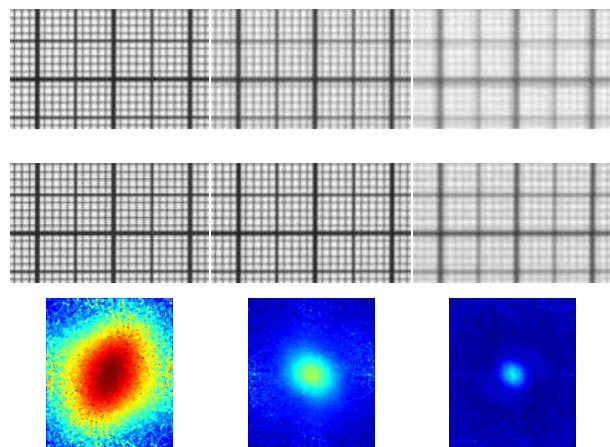

Fig. 5. Top to bottom: original frame, deconvolved frame, MTF ($\lambda_{\mathrm{sel}}/\lambda_{\mathrm{ref}}$); left to right: λ_{sel}=500nm, 650nm, 700nm, λ_{ref}=550nm.

Fig. 5 presents the results of calibration and deconvolution for three spectral channels with varying blurring PSFs. The PSFs and MTFs are derived from the blockwise analysis introduced in Fig. 4. The images in the second row of the fig-

ure are derived by deconvolution of the original frames in the first row with the corresponding PSFs in the same column.

As usual when visualizing multispectral images, the multispectral images are transformed to the RGB domain using a linear transformation [2] and gamma correction (see top row of Fig. 6). The left image depicts the result without applying any geometrical corrections, leaving rainbow-like color artifacts. When correcting the transversal aberrations according to [4], i.e., when the spectral channels are registered, the main artifacts are removed, but still a certain degree of color content of the black/white object remains. By application of the proposed algorithm, the remaining color fringes are practically eliminated and the image is sharper and exhibits more contrast, as it can be seen from the profile plots. The bottom row of Fig. 6 shows the differences between the red and green color channels. In the ideal case without distortions, there should be no differences since we acquired a grayscale template. The remaining differences indicate the amount of misregistration and difference in the PSF. The number in the top of each differential image denotes the variance of each one relative to the power of the corresponding color channels. It can be seen that the difference between the color channels can be greatly reduced by applying registration and deconvolution.
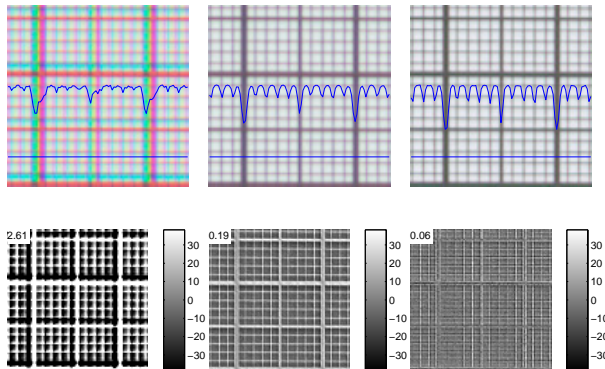

Fig. 6. Top: Crops of reconstructed RGB images with a profile plot (unregistered, registered, deconvolved image); bottom: difference between red and green channel, the numbers indicate the variance relative to the image power.

5. CONCLUSIONS

We have derived a physical explanation for the longitudinal aberrations caused by the optical bandpass filters in a multispectral filter-wheel camera. At the basis of this model, we modeled the aberration as a shift-variant, non-symmetrical, off-centered PSF. Our calibration algorithm enables a blockwise estimation of the PSF. The deconvolution is also performed blockwise, while blocking artifacts are suppressed by crossfading. The resulting image shows less color fringes and is sharper and has stronger contrast.

In our future work, we plan to integrate the compensation of transversal aberrations (geometrical distortions) into the deconvolution process to simplify the model and the complexity of the compensation algorithm.

6. REFERENCES

[1] F. König and Patrick G. Herzog, "On the limitation of metameric imaging," *Proc. IS&T´s PICS*, vol. 2, pp. 163–168, 1999.

[2] St. Helling, E. Seidel, and W. Biehlig, "Algorithms for spectral color stimulus reconstruction with a seven-channel multispectral camera," in *IS&Ts CGIV*, Aachen, Germany, Apr 2004, pp. 254–258.

[3] Philippe Colantoni, Ruven Pillay, Christian Lahanier, and Denis Pitzalis, "Analysis of multispectral images of paintings," in *Proc. EUSIPCO*, Florence, Italy, Sep 2006.

[4] Johannes Brauers, Nils Schulte, and Til Aach, "Modeling and compensation of geometric distortions of multispectral cameras with optical bandpass filter wheels," in *Proc. EUSIPCO*, Poznań, Poland, Sep 2007, pp. 1902–1906.

[5] V. Cappellini, A. Del Mastio, A. De Rosa, A. Piva, A. Pelagotti, and H. El Yamani, "An automatic registration algorithm for cultural heritage images," in *IEEE ICIP*, Genova, Italy, Sep 2005, vol. 2, pp. II–566–9.

[6] Filip Šroubek, Gabriel Cristóbal, and Jan Flusser, "A unified approach to superresolution and multichannel blind deconvolution," *IEEE TIP*, vol. 16, no. 9, pp. 2322–2332, Sep 2007.

[7] Gulcin Caner, A. Murat Tekalp, Gaurav Sharma, and Wendi Heinzelman, "Local image registration by adaptive filtering," *IEEE TIP*, vol. 15, no. 10, pp. 3053–3065, Oct 2006.

[8] A. Mansouri, F. S. Marzani, J. Y. Hardeberg, and P. Gouton, "Optical calibration of a multispectral imaging system based on interference filters," *SPIE Opt. Eng.*, vol. 44, no. 2, pp. 027004.1–027004.12, Feb 2005.

[9] Warren J. Smith, *Modern Optical Engineering*, McGraw-Hill, 2000.

[10] Rafael C. Gonzalez and Richard E. Woods, *Digital Image Processing (3rd Edition)*, Prentice-Hall, Inc., Upper Saddle River, New Jersey, USA, 2006.